A Comparison of Computational Complexities of HFEM and ABC Based Finite Element Methods†

Muhammad A. Nasir and Weng Cho Chew
Department of Electrical and Computer Engineering
University of Illinois, Urbana, IL 61801

Padma Raghavan and Michael T. Heath
NCSA and Department of Computer Science
University of Illinois, Urbana, IL 61801

Keywords: Hybrid Finite Element Method (HFEM), Surface Integral Equation Radiation Boundary Conditions, Matrix Partitioning, Nested Dissection

Abstract

The solution of a hybrid finite element method (HFEM) problem is considered. It is shown that a suitable ordering of the FEM mesh results in a canonical HFEM matrix system. This linear system can be solved in $O(N^{1.5})$ cost when sparse direct methods are used. This cost is comparable to FEM methods using approximate boundary conditions and a similar sparse solution method.

I. Introduction

Surface integral equations have been used in the past as boundary conditions for electromagnetic problems. Their use as a boundary condition was first reported in the work of McDonald and Wexler [1]. When surface integral equations are used as boundary conditions for FEM, the method is called the hybrid finite element method (HFEM). Researchers have used this method to solve open-region electromagnetic scattering problems [2, 3]. Sparse linear systems associated with an FEM formulation typically have nonzeros clustered within a small band along the diagonal. Sparse direct solvers can exploit this property to lead to low computation cost. However, a straightforward application of surface integral equations to an FEM matrix destroys its *banded* nature, making infeasible the use of *banded* direct solvers to achieve low computational cost.

As a consequence, there has been a fair amount of research directed towards preserv-

† This work is supported by Office of Naval Research under grant N000-14-89-J1286, the Army Research Office under contract DAAL03-89-G0339, and the National Science Foundation under grant NSF ECS 92-2446 6.

ing the banded form of open-region problems through the use of approximate boundary conditions. These boundary conditions model the behavior of the field extending to infinity on the outer boundary of the finite region. These approximate boundary conditions are mainly absorbing boundary conditions (ABC) [4, 5, 6, 7, 8] and on-surface radiation conditions (OSRC) [9] used to approximate the radiation boundary condition. When these methods are applied correctly, the solution inside the truncated region approximates the problem over the entire space. However, these methods have drawbacks. Some of them impose restrictions on the shape of outer boundary and/or shape of the scatterer, while others are sensitive to the distance between the outer boundary and the scatterer. For the purpose of clarity we shall refer to all methods based on approximate boundary conditions as FEM–ABC.

It was noted by Jin and Liepa [10] that solving the HFEM problem in a certain order resulted in considerable speedup over straightforward implementation of HFEM. However, no quantitative estimates of this speedup were presented. We use a mathematically equivalent variation of [10] in which instead of changing the order of solution we order the FEM mesh in a certain way. Ordering the mesh in this way produces a canonical HFEM matrix. This canonical form is easy to solve and is well suited for an analysis of the computational complexity of the solution. In order to distinguish this modified form of HFEM from a straightforward implementation, HFEM we shall call it ordered hybrid finite element method (OHFEM). When the linear system produced by OHFEM is partitioned and solved by applying sparse techniques the operation count is reduced to $O(N^{1.5})$, which is the cost of solving FEM with an absorbing boundary condition (FEM–ABC), where N is the number of unknowns in the problem. It is also shown that contrary to common belief, the computational effort required for the part resulting from the surface integral equations is not the dominant cost in the overall solution.

A brief formulation of the problem is described in Section II, followed by a note on mesh ordering in Section III. Section IV presents an analysis of the cost of solving OHFEM.

Section V provides a comparison of empirical computational costs of OHFEM and FEM–ABC. Section VI provides numerical results for validation, and Section VII draws some interesting conclusions based on this scheme.

II. Formulation

We consider the 2.5-D problem of scattering of a plane wave from a 2-D dielectric cylinder of arbitrary shape. The plane wave is incident at an oblique angle to the cylinder axis. Figure 1 illustrates the geometry of this problem. The inhomogeneous dielectric cylinder can have frequency and/or loss dispersion in addition to being both electrically and magnetically anisotropic. On an FEM mesh, boundaries Γ_c, Γ_b, and Γ_o are one discretization point apart. The problem is divided into two regions: the source-free inhomogeneous region inside the boundary Γ_o, and the homogeneous region outside the scatterer. Inside Γ_o, $\boldsymbol{E}_s$ formulation [11] is used. In this region the transverse field is governed by

$$\overline{\boldsymbol{\mu}}_s \cdot \hat{z} \times \nabla_s \times \nu_{zz} \nabla_s \times \boldsymbol{E}_s - \hat{z} \times \kappa_{zz} \nabla_s \cdot \overline{\boldsymbol{\epsilon}}_s \cdot \boldsymbol{E}_s - \omega^2 \overline{\boldsymbol{\mu}}_s \cdot \hat{z} \times \overline{\boldsymbol{\epsilon}}_s \cdot \boldsymbol{E}_s + k_z^2 \hat{z} \times \boldsymbol{E}_s = 0, \quad (1)$$

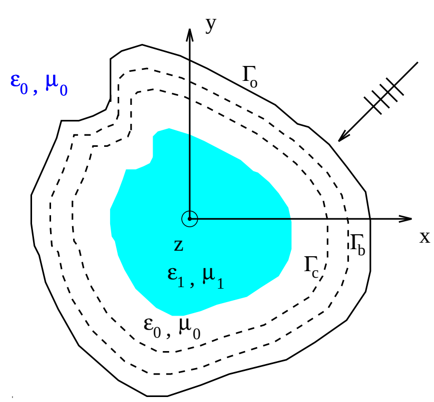

Figure 1 Geometry of an arbitrary dielectric scatterer showing different boundaries.

where $(\overline{\boldsymbol{\mu}}_s, \overline{\boldsymbol{\epsilon}}_s)$ are transverse parts of $(\overline{\boldsymbol{\mu}}, \overline{\boldsymbol{\epsilon}})$ and are uncoupled from their longitudinal parts $(\mu_{zz}, \epsilon_{zz})$. The scatterer is uniform in z, and $e^{ik_z z}$ dependence is assumed. Equation (1) can be written in a compact operator form as,

$$\mathcal{L}_e \cdot \boldsymbol{E}_s + k_z^2 \mathcal{B} \cdot \boldsymbol{E}_s = 0. \quad (2)$$

Defining the inner product $\langle \boldsymbol{A}_s, \boldsymbol{B}_s \rangle = \int_S dS \boldsymbol{A}_s \cdot \boldsymbol{B}_s$, Equation (2) may be tested with $\widetilde{\boldsymbol{H}}_s$ to give

$$\langle \widetilde{\boldsymbol{H}}_s, \mathcal{L}_e \cdot \boldsymbol{E}_s \rangle + k_z^2 \langle \widetilde{\boldsymbol{H}}_s, \mathcal{B} \cdot \boldsymbol{E}_s \rangle = 0, \tag{3}$$

where $\widetilde{\boldsymbol{H}}_s$ is the magnetic field solution in the transposed medium $(\overline{\boldsymbol{\mu}}^t, \overline{\boldsymbol{\epsilon}}^t)$. Equation (3) can be shown to be variational [11]. FEM is used to obtain the matrix equation

$$\overline{\boldsymbol{A}} \cdot \boldsymbol{a} = 0, \tag{4}$$

where the elements of matrix $\overline{\boldsymbol{A}}$ are given by

$$[\ \overline{\boldsymbol{A}}\ ]_{mn} = \langle \widetilde{\boldsymbol{H}}_{ms}, (\mathcal{L}_e + k_z^2 \mathcal{B}) \cdot \boldsymbol{E}_{ns} \rangle. \tag{5}$$

Equation (4) can be arranged in a more suggestive form

$$\begin{pmatrix} \overline{\boldsymbol{A}}_{ii} & \overline{\boldsymbol{A}}_{ib} & \overline{0} \\ \overline{\boldsymbol{A}}_{bi} & \overline{\boldsymbol{A}}_{bb} & \overline{\boldsymbol{A}}_{bo} \\ 0 & \overline{\boldsymbol{A}}_{ob} & \overline{\boldsymbol{A}}_{oo} \end{pmatrix} \begin{pmatrix} \boldsymbol{a}_i \\ \boldsymbol{a}_b \\ \boldsymbol{a}_o \end{pmatrix} = \begin{pmatrix} 0 \\ 0 \\ 0 \end{pmatrix}, \tag{6}$$

where $\boldsymbol{a}_i$ are the unknowns inside the boundary Γ_b, $\boldsymbol{a}_b$ are the unknowns on the boundary Γ_b, and $\boldsymbol{a}_o$ are the unknowns on the boundary Γ_o.

In the homogeneous region, the field components are decoupled. Therefore, we can use a scalar ϕ to represent either of the two field components. The field at any point outside Γ_b can be expressed in terms of the field on the boundary Γ_b through the surface integral equation,

$$\phi(\boldsymbol{r}) = \phi_{inc}(\boldsymbol{r}) - \int_{\Gamma_b} dl' \hat{n}' \cdot [\ g_o(\boldsymbol{r}, \boldsymbol{r}') \nabla' \phi(\boldsymbol{r}') - \phi(\boldsymbol{r}') \nabla' g_o(\boldsymbol{r}, \boldsymbol{r}')\ ],$$
$$\Gamma_b \in \mathbb{R}^2, \{\boldsymbol{r} \in \mathbb{R}^3 : \sqrt{|\ \Gamma_b\ | + z^2} < |\ \boldsymbol{r}\ | \leq\ \infty\}. \tag{7}$$

Consequently, unknowns at the outer boundary Γ_o can be related to the unknowns at Γ_b. In matrix notation

$$\overline{\boldsymbol{b}} \boldsymbol{\phi}_o = \overline{\boldsymbol{g}} \boldsymbol{\phi}_b + \boldsymbol{\phi}_{inc}, \tag{8}$$

where $\boldsymbol{\phi}_o$ and $\boldsymbol{\phi}_b$ are the discretized versions of the scalar field component on Γ_o and Γ_b respectively. For both field components

$$\overline{\boldsymbol{B}} \boldsymbol{a}_o = \overline{\boldsymbol{G}} \boldsymbol{a}_b + \boldsymbol{a}_{inc}. \tag{9}$$

Equation (9) is used to eliminate $\boldsymbol{a}_o$ from Equation (6), giving the final equation

$$\begin{pmatrix} \overline{\boldsymbol{A}}_{ii} & \overline{\boldsymbol{A}}_{ib} \\ \overline{\boldsymbol{A}}_{bi} & \widetilde{\boldsymbol{G}} \end{pmatrix} \begin{pmatrix} \boldsymbol{a}_i \\ \boldsymbol{a}_b \end{pmatrix} = \begin{pmatrix} 0 \\ \tilde{\boldsymbol{a}}_{inc} \end{pmatrix}, \tag{10}$$

where $\widetilde{\boldsymbol{G}} = (\overline{\boldsymbol{A}}_{bb} + \overline{\boldsymbol{A}}_{bo}\overline{\boldsymbol{B}}^{-1}\overline{\boldsymbol{G}})$ and $\tilde{\boldsymbol{a}}_{inc} = -(\overline{\boldsymbol{A}}_{bo}\overline{\boldsymbol{B}}^{-1}\boldsymbol{a}_{inc})$.

III. Mesh Ordering

Although in Equation (6) the unknowns inside Γ_b, on Γ_b, and on Γ_o appear grouped together, in practice it is seldom the case. When Equation (9) is applied in a straightforward manner to the matrix Equation (6), the resulting matrix can have its bandedness completely destroyed. Figures 2 and 3 show an FEM matrix before and after the surface integral equation has been applied to it. It is obvious that the bandedness has been completely destroyed. When solving this matrix, fill-ins (original zeros that become nonzeros) will almost certainly cause it to become a dense matrix. This result is fundamentally contrary to the spirit of FEM. With such matrices, it is common to see operation counts of $O(N^3)$. This is the single most serious shortcoming in an otherwise promising method.

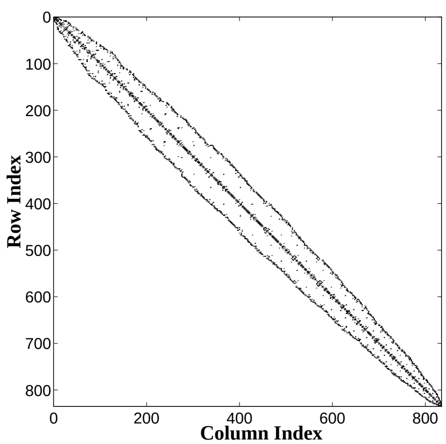

Figure 2 Zero/Non-zero structure of the FEM matrix.

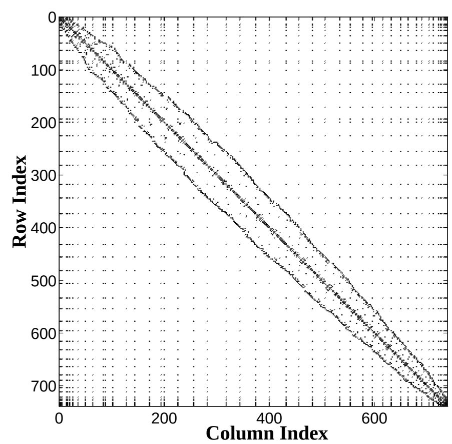

Figure 3 Zero/Non-zero structure of the HFEM matrix.

Previously, we had proposed an $O(N^2)$ solution scheme [12]. The scheme in [12] employed an ordering that resulted in a canonical matrix shown in Figure 5 of [12] reproduced below as Figure 4. The mesh was ordered by labeling the unknowns on Γ_b and Γ_o last. This matrix form was more suitable for solution through matrix partitioning, and the structure of the matrix was such that it could be easily analyzed for computational complexity. The submatrices generated by the partitioning of the canonical matrix in Figure 4 are shown in Figure 5. However, in matrices $\overline{\boldsymbol{A}}_{12}$ and $\overline{\boldsymbol{A}}_{21}$, the nonzeros were peppered all over the columns. As a consequence, even if we could find an $O(N^{1.5})$ LU decomposition of $\overline{\boldsymbol{A}}_{11}$ and inverse of $\overline{\boldsymbol{A}}_{22}$ in Equation (12) (next section) we could not find the product $\overline{\boldsymbol{A}}_{11}^{-1}\,\overline{\boldsymbol{A}}_{12}$ in less than $O(N^2)$. Therefore, the overall cost of solution was dominated by the cost of this matrix product.

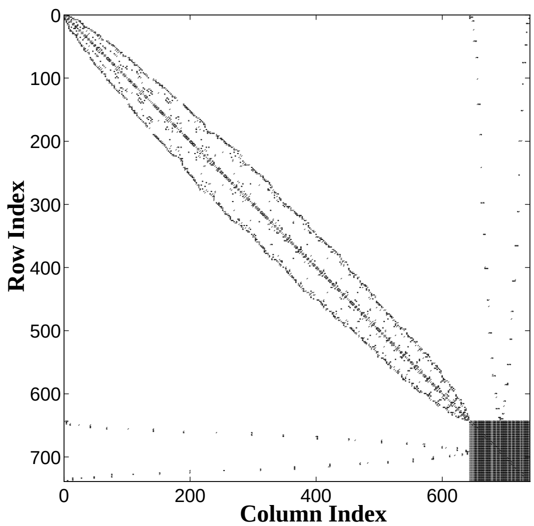

Figure 4 OHFEM matrix [12].

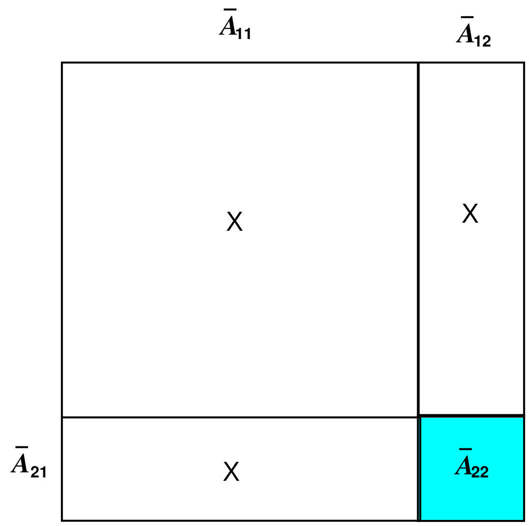

Figure 5 Partitioned OHFEM matrix [12].

With the purpose of removing this bottleneck, we propose a new mesh ordering that is not only easy to implement, but also generates a canonical matrix in which the product $\overline{\boldsymbol{A}}_{11}^{-1}\,\overline{\boldsymbol{A}}_{12}$ can be computed in $O(N^{1.5})$, leading to an overall complexity of $O(N^{1.5})$. The FEM mesh is ordered in four steps: (1) the region inside Γ_c is meshed to generate an $(N-2m)$ system with the unknowns numbered in the range $1, \cdots, (N-2m)$, where m is the number of unknowns on each of Γ_c, Γ_b, and Γ_o, (2) nodes on Γ_c are numbered contiguously, beginning with $(N-2m+1)$ and ending at $(N-m)$, (3) nodes on Γ_b are numbered in a similar fashion, this time starting with $(N-m+1)$ and ending at N, and

(4) last m nodes on Γ_o are numbered contiguously. This ordering results in the HFEM matrix shown in Figure 6. This matrix can be partitioned according to Figure 7 in which symbol Θ denotes zeroes, symbol X denotes sparse submatrices, and the blank submatrices denote sparse banded structures.

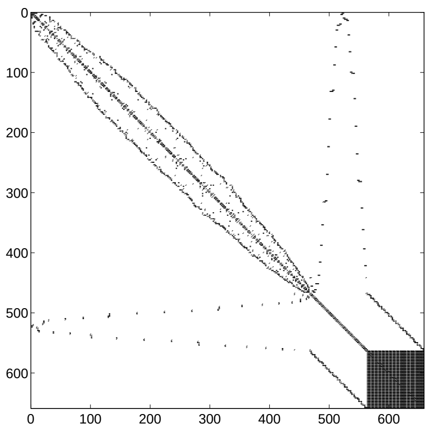

Figure 6 OHFEM matrix.

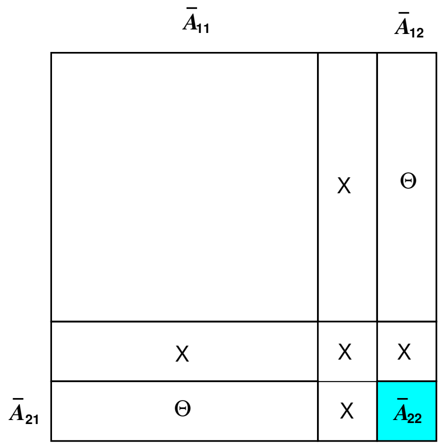

Figure 7 Partitioned OHFEM matrix.

IV Computational Complexity

In this section we derive an expression for the computational cost of the OHFEM formulation. The partitioned OHFEM matrix can be written as:

$$\begin{pmatrix} \overbrace{\overline{\boldsymbol{A}}_{11}}^{n\times n} & \overbrace{\overline{\boldsymbol{A}}_{12}}^{n\times m} \\ \underbrace{\overline{\boldsymbol{A}}_{21}}_{m\times n} & \underbrace{\overline{\boldsymbol{A}}_{22}}_{m\times m} \end{pmatrix} \begin{pmatrix} \boldsymbol{a}_1 \\ \boldsymbol{a}_2 \end{pmatrix} = \begin{pmatrix} \mathbf{o} \\ \boldsymbol{b} \end{pmatrix}; \; n = (N - m), \tag{11}$$

where $\overline{\boldsymbol{A}}_{ij}$ is defined in Figure 7. The solution process involves computing $\boldsymbol{a}_1$ and $\boldsymbol{a}_2$ using:

$$\boldsymbol{a}_1 = -\overline{\boldsymbol{A}}_{11}^{-1}\overline{\boldsymbol{A}}_{12}\,(\,\underbrace{\overline{\boldsymbol{A}}_{22} - \overline{\boldsymbol{A}}_{21}\overline{\boldsymbol{A}}_{11}^{-1}\overline{\boldsymbol{A}}_{12}}_{\widetilde{\boldsymbol{A}}}\,)^{-1}\cdot\boldsymbol{b}, \qquad \text{and} \qquad \boldsymbol{a}_2 = \widetilde{\boldsymbol{A}}^{-1}\,\boldsymbol{b}. \tag{12}$$

The value of m, the number of surface unknowns on the boundary Γ_b, is typically a small constant c_0 times $N^{1/2}$. The matrices $\overline{\boldsymbol{A}}_{11}$, $\overline{\boldsymbol{A}}_{12}$, and $\overline{\boldsymbol{A}}_{21}$ are sparse, while the matrix $\overline{\boldsymbol{A}}_{22}$ is dense. Furthermore, the leading $(n - m) \times m$ submatrix of $\overline{\boldsymbol{A}}_{12}$ and the leading

$m \times (n-m)$ submatrix of $\overline{\boldsymbol{A}}_{21}$ are both zero; this fact can be used to reduce computational cost.

A suitable sparsity preserving LU decomposition of $\overline{\boldsymbol{A}}_{11}$ is central to the solution process. In such a decomposition the matrix is permuted so that that the matrix factors $\overline{\boldsymbol{L}}_{11}$ and $\overline{\boldsymbol{U}}_{11}$ are sparse and are computed at the expense of low arithmetic costs. We also restrict the sparsity preserving permutation to one in which the m unknowns corresponding to Γ_c are numbered last in the range $(n-m), \cdots, n$. Since the matrix $\overline{\boldsymbol{A}}_{11}$ corresponds to a 2-D FEM mesh, its *graph* satisfies a $n^{1/2}$ separator theorem [13], and generalized nested dissection can be applied effectively to permute the leading $(n - m) \times (n - m)$ submatrix to preserve sparsity. The methods described in [14] can be used to compute the LU factors of $\overline{\boldsymbol{A}}_{11}$ using $cost_{LU} = d_0 n^{1.5}$ arithmetic operations, where d_0 is a constant. It is also known that the number of nonzeroes in the two factors, $nonz_{LU}$, is $d_1 n \log n$, where d_1 is a constant; this number reflects the cost of solving triangular systems represented in terms of the factors.

Now we estimate the cost of computing $\boldsymbol{a}_2$, which requires computing $\widetilde{\boldsymbol{A}}^{-1}$ and forming the product $\widetilde{\boldsymbol{A}}^{-1}\, \boldsymbol{b}$:

1. The product $\overline{\boldsymbol{A}}_{11}^{-1}\, \overline{\boldsymbol{A}}_{12}$ can be evaluated by solving the system $\overline{\boldsymbol{A}}_{11}\, \boldsymbol{x} = \boldsymbol{r}$, m times, for $\boldsymbol{r}$ corresponding to each of the m columns of $\overline{\boldsymbol{A}}_{12}$. Recall that the first $(n-m)$ values in each column of $\overline{\boldsymbol{A}}_{12}$ are zero. Given the LU factors of $\overline{\boldsymbol{A}}_{11}$ each triangular solution after the first would cost m^2 operations with the first one of cost $nonz_{LU}$; the cost for this step is therefore $nonz_{LU} + m^3$.
2. Observe that since the leading $(n-m) \times m$ submatrix of $\overline{\boldsymbol{A}}_{12}$ and the leading $m \times (n-m)$ submatrix of $\overline{\boldsymbol{A}}_{21}$ are both zero, only trailing $m \times m$ submatrices of $\overline{\boldsymbol{A}}_{21}$ and $\overline{\boldsymbol{A}}_{11}^{-1}\, \overline{\boldsymbol{A}}_{12}$ need be multiplied. The cost of such a multiplication is m^3.
3. The required matrix subtraction to compute $\widetilde{\boldsymbol{A}}$ costs m^2, and matrix inversion (of a dense matrix $\widetilde{\boldsymbol{A}}$) in turn requires $(4/3)m^3$ operations.

4. Finally, solving for $\boldsymbol{a}_2$ requires an additional m^2 operations.

Computing $\boldsymbol{a}_1$ from $\boldsymbol{a}_2$ requires m^2 operations for the matrix vector product followed by another $nonz_{LU}$ operations for the triangular solution. Table I presents a summary of the computational cost; $nonz_{LU}$ is specified as $d_1 n \log n$.

TABLE I
SUMMARY OF COST OF COMPUTATION

STEP	OPERATION COUNT
Computing LU factors of $\overline{\boldsymbol{A}}_{11}$	$d_0\ n^{1.5}$
Computing $\boldsymbol{a}_2$	$d_1\ n\ \log n\ + \frac{10}{3}\ m^3\ + 2\ m^2$
Computing $\boldsymbol{a}_1$	$d_1\ n\ \log n\ + m^2$
TOTAL	$d_0\ n^{1.5}\ +\ \frac{10}{3}\ m^3\ + 2\ d_1\ n\ \log n\ +\ 3\ m^2$

Since $n < N$ and $m = c_0 N^{0.5}$ the total cost is:

$$\text{cost}\ \leq d_0\ N^{1.5} + \frac{10}{3} c_0^3 N^{1.5} + d_1\ N\ \log N\ +\ 3\ c_0^2\ N. \tag{13}$$

From the above discussion, it follows that in the order of magnitude sense, the cost of OHFEM formulation is the same as that of the FEM–ABC formulation when nested dissection based methods are used. However, typically the number of unknowns is smaller for the OHFEM formulation for a given problem. As a consequence, the costs of our method compare very favorably with that for FEM–ABC as demonstrated by our experiments in the next section.

V Empirical Computational Costs

To demonstrate the viability of the OHFEM formulation, we empirically compare the solution cost to that of FEM–ABC for a set of four problems. In each problem, circular cylindrical dielectric scatterers of increasing electrical size are chosen. For FEM–ABC, the outer boundary is maintained at one wavelength from the scatterers. Also, for the sake of objective comparison, the mesh shape and discretization size are kept as even as possible. It is perhaps worthwhile to point out that a geometry with a convex hull is chosen intentionally because choosing an arbitrary geometry—an airplane, for example—will increase the size of the FEM–ABC problem inordinately compared to OHFEM; for such cases FEM–ABC may not even remain a viable option. For each problem, we generated two versions, one suitable for the OHFEM formulation and another suitable for the FEM–ABC method. The total number of unknowns for each version and m, the number on the boundary Γ_b for the OHFEM formulation are given in Table II.

TABLE II

Description of Problem Parameters for Both Formulations

LABEL	OHFEM size	OHFEM m	FEM–ABC size
P1	562	96	10,850
P2	3,058	176	16,226
P3	11,698	336	28,802
P4	26,002	464	47,234

We solved each problem by two methods. The first method used is based on a nested dissection heuristic to compute the LU factorization. More specifically the nested dissection heuristic used is that of Sparspak [15, 16] in the context of work in [14]. For the OHFEM formulation, as described earlier, the nested dissection ordering is not allowed to permute the last m unknowns. Such a restriction is obviously not imposed for the FEM–ABC formulations. The values of $cost_{LU}$ and $nonz_{LU}$ are observed for each version of each problem. These costs are worst case values to account for extra arithmetic work that could result from pivoting for numeric stability in the course of computing the decomposition. Although the nested dissection heuristic used is not guaranteed to compute optimal separators, in practice it does well in the asymptotic sense. In Table III we present the overall cost of the solution process for either method using the observed values of $cost_{LU}$ and $nonz_{LU}$ for the corresponding problem formulation. For the OHFEM formulation these costs are used in Equation (13) to compute total costs. Observe that the OHFEM formulation has the overall lower cost.

TABLE III

Operation count (in millions) using sparse *LU* factorization based on nested dissection

LABEL	OHFEM	FEM–ABC
P1	7.61	351.2
P2	114.2	738.8
P3	854.3	1,827.1
P4	3,443.9	4,130.9

We next compared the costs using sparse *LU* decomposition based on a general purpose sparsity preserving heuristic called Multiple Minimum Degree [15, 16]. Although no bounds have been proved for the arithmetic cost using this ordering heuristic, in practice it performs better than nested dissection heuristics. We compute the *LU* factorization based on this heuristic and an implementation in Matlab [17]. Once again the total solution cost is presented for either formulation in Table IV. Again, the OHFEM formulation is observed to have lower cost.

TABLE IV

Operation count (in millions) using sparse *LU* factorization based on multiple minimum degree heuristic

LABEL	OHFEM	FEM–ABC
P1	7.31	187.2
P2	76.6	389.2
P3	731.8	1,236.1
P4	2,591.4	3,282.9

We had shown earlier by careful formulation and analysis of the solution process that both the OHFEM and FEM–ABC formulations have the same asymptotic computational complexity. Our empirical results substantiate this. Furthermore, because a comparable version of the same problem is of much larger size for the FEM–ABC formulation, the solution costs for our OHFEM approach tend to be smaller by a constant factor.

VI Numerical Results

To validate OHFEM, two test cases were considered. First, the problem of scattering of a TM mode incident on a circular cylinder was considered. The dielectric cylinder has an ϵ_r=2.0. The TM mode was obliquely incident at an angle of 45° to the z-axis. The cylinder had a radius of $.33\lambda_o$. Figures 8 and 9 compare the E_ρ and E_ϕ components of the scattered field with the closed form series solution. The agreement is excellent. The problem had a total of 834 unknowns. It took roughly 60 seconds to solve it on a SparcStation 2, and about 2.3 seconds on a Cray-YMP.

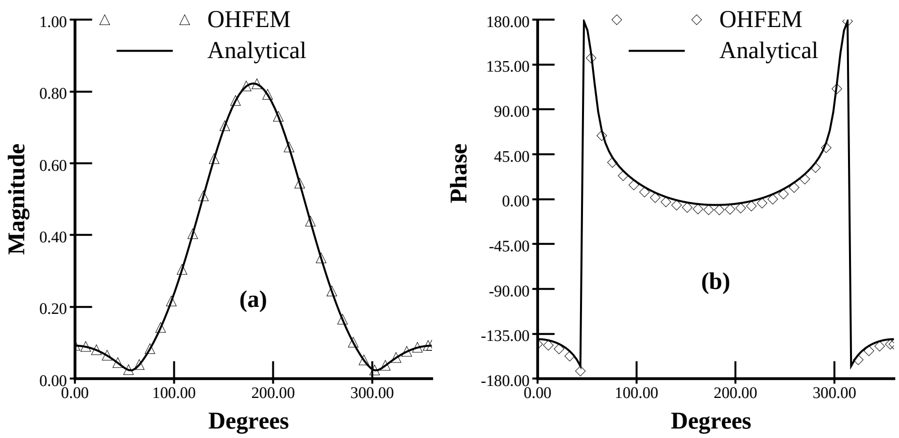

Figure 8 E_ρ component of the scattered field. (a) Magnitude (b) Phase in degrees.

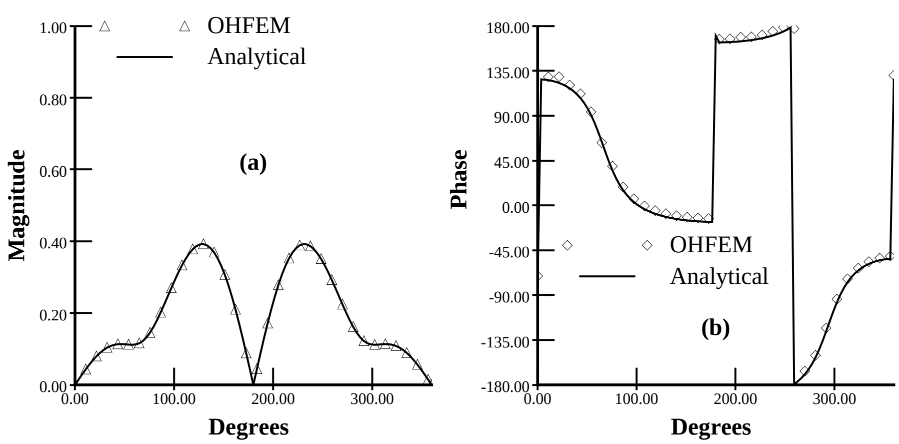

Figure 9 E_ϕ component of the scattered field. (a) Magnitude (b) Phase in degrees.

Next, scattering from square dielectric cylinder is calculated when a TE plane wave is incident on it normally. The scatterer has a side length of $.33\lambda_o$, and $\epsilon_r = 2.0$. Figure 10 compares the results of OHFEM with those of EBC [18] method and NEPAL (Nested Equivalence Principle Algorithm)[19, 20]. It may be noted that there is a very good agreement between T-matrix algorithm of [21] and the EBC method.

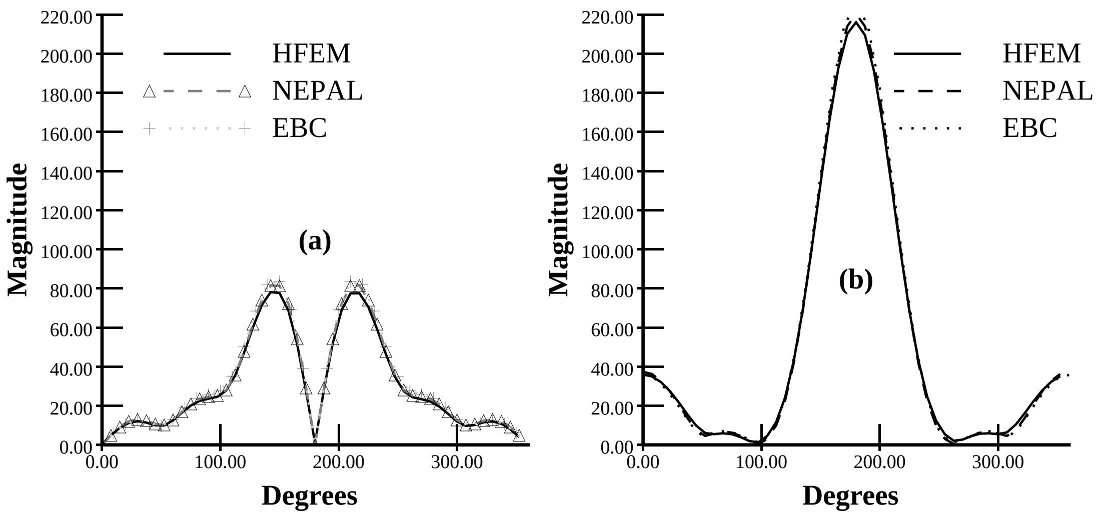

Figure 10 Scattered field from a rectangular scatterer. (a) Magnitude of E_y (b) Magnitude of E_x

VII Conclusions

We have demonstrated that mesh ordering is crucial to the success of HFEM as a viable method of solving open-region scattering problems. If implemented properly, the cost of computation of OHFEM is no more than that of the other methods of approximating the radiation boundary condition when goemetries with a convex hull are used; when the geometries are arbitrary, FEM–ABC may become unsuitable due to an inordinately large number of unknowns. The OHFEM solution is “exact”, except for discretization errors. There are no restrictions on the shape of the scatterer, the shape of the outer boundary, or the distance between the scatterer and the outer boundary. It is hoped that this observation will help promote the use of the surface integral equation as a boundary condition for FEM.

VIII References

[1] B. McDonald and A. Wexler, "Finite element solution of unbounded field problems," *IEEE Trans. Microwave Theory Tech.*, vol. MTT-20, pp. 841–847, December 1972.

[2] J. Jin and V. V. Liepa, "Application of hybrid finite element method to electromagnetic scattering from coated cylinders," *IEEE Antennas Propagat.*, vol. AP-36, no. 10, pp. 50–54, January 1988.

[3] O. M. Ramahi and R. Mittra, "A surface integral equation method for the finite element solution of waveguide discontinuity problems," *IEEE Trans. Microwave Theory Tech.*, vol. MTT-39, no. 3, pp. 604–608, March 1991.

[4] O. M. Ramahi, A. Khebir, and R. Mittra, "Numerically derived absorbing boundary condition for the solution of open-region scattering problem," *IEEE Antennas Propagat.*, vol. AP-39, no. 3, pp. 350–354, March 1991.

[5] A. Bayliss and E. Turkel, "Boundary conditions for the numerical solution of elliptic equations in exterior regions," *SIAM J. Appl. Math.*, vol. 42, no. 2, pp. 430–451, April 1982.

[6] B. Engquist and A. Majda, "Radiation boundary conditions for the numerical simulation of waves," *Math. Comput.*, vol. 31, no. 139, pp. 629–651, July 1977.

[7] Z. P. Liao, H. L. Wong, B. P. Yang, and Y. F. Yuan, "A transmitting boundary for transient wave analysis," *Sci. Sin. Ser. A (China)*, vol. 27, no. 10, pp. 1063–1076, 1984.

[8] R. L. Higdon, "Absorbing boundary conditions for difference approximations to the multi-dimensional wave equations," *Math Comput.*, vol. 47, no. 176, pp. 437–459, October 1986.

[9] G. A. Kriegsman, A. Taflove, and K. R. Umashankar, "A new formulation of electromagnetic wave scattering using an on surface radiation boundary condition approach," *IEEE Antennas Propagat.*, vol. AP-35, no. 2, pp. 152–161, February 1987.

[10] J. Jin and V. V. Liepa, "A note on hybrid finite element method for solving scattering problems," *IEEE Antennas Propagat.*, vol. AP-36, no. 10, pp. 1486–1489, October 1988.

[11] W. C. Chew and M. A. Nasir, "A variational analysis of anisotropic, inhomogeneous dielectric waveguides," *IEEE Trans. Microwave Theory Tech.*, vol. MTT-37, no. 4, pp. 661–668, April 1989.

[12] M. A. Nasir and W. C. Chew, "Scattering from dielectric cylinders:$\boldsymbol{E}_s$ formulation, using a combination of FEM and integral equation approach," *IEEE Antennas Propagat. Int. Symp. Digest*, vol. 3, pp. 1772–1775, July 1993.

[13] R. J. Lipton, D. J. Rose, and R. E. Tarjan, "Generalized nested dissection," *SIAM J. Numerical Anal.*, vol. 16, pp. 346–358, 1979.

[14] J. George and E.-Y. Ng, "On the complexity of sparse LU and QR factorization of finite element matrices," *SIAM J. Sci. Stat. Comput.*, vol. 9, pp. 849–861, 1988.

[15] E. Chu, A. George, J. Liu, and E. Ng, *Sparspak: Waterloo Sparse Matrix Package User's Guide for Sparspak-A.* Department of Computer Science, University of Waterloo, Waterloo, Ontario, Canada, 1984.

[16] A. George and E. Ng, *Sparspak: Waterloo Sparse Matrix Package User's Guide for Sparspak-B.* Department of Computer Science, University of Waterloo, Waterloo, Ontario, Canada, 1984.

[17] J. R. Gilbert, C. Moler, and R. Schreiber, "Sparse matrices in MATLAB: Design and implementation," *SIAM J. Mat. Anal. and Appl.*, vol. 13, pp. 333–356, 1992.

[18] R. L. Wagner, "Multiple scattering by square dielectric cylinders and three-dimensional finite-difference time-domain modeling of a subsurface interface radar system," M.S. thesis, University of Illinois, Urbana, 1991.

[19] W. Chew and C. Lu, "The use of Huygens' equivalence principle for solving the volume integral equation of scattering," *IEEE Trans. Microwave Theory Tech.*, vol. 41, no. 7, pp. 897–904, July 1993.

[20] W. Chew and C. Lu, "NEPAL–an algorithm for solving the volume integral equation," *Micro. Opt. Tech. Lett.*, vol. 6, no. 3, pp. 185–188, March 1993.

[21] W. C. Chew *et al.*, "A generalized recursive algorithm for wave scattering solutions in two dimensions," *IEEE Trans. Microwave Theory Tech.*, vol. 40, no. 4, pp. 716–723, April 1992.